Supporting Information

Carvalho et al. 10.1073/pnas.1221524110

SI Materials and Methods

Lipids and Reagents. Chemicals were purchased from Sigma-Aldrich unless specified otherwise. L-α-Phosphatidylcholine (EPC) and 1,2-distearoyl-sn-glycero-3-phosphoethanolamine-*N*-[biotinyl polyethylene glycol 2000] (biotinylated lipids), 1,2-dioleoyl-sn-glycero-3-phosphocholine (DOPC), 1,2-dipalmitoyl-sn-glycero-3-phosphoethanolamine-*N*-[methoxy(polyethylene glycol)-2000] (PEG-PE with a 2-kDa polyethylene glycol tail), the fluorescently labeled lipid 1,2-dioleoyl-sn-glycero-3-phosphoethanolamine-*N*-(lissamine rhodamine B sulfonyl) (rhodamine-PE), and the biotinylated lipid 1,2-dipalmitoyl-sn-glycero-3-phosphoethanolamine-*N*-(cap biotinyl) (biotin-PE) were purchased from Avanti polar lipids. Fluorescently labeled Pacific Blue 1,2-ditetradecanoyl-sn-glycero-3-phosphoethanolamine lipids (Pacific Blue-PE) and neutravidin were purchased from Invitrogen.

Proteins. Actin was either purchased from Cytoskeleton and used with no further purification or purified in-house from rabbit skeletal muscle by standard procedures including a gel filtration on a Sephacryl S-200 high-resolution column (GE Healthcare) (1). Fluorescent Alexa 488 actin was obtained from Molecular Probes or prepared by labeling amine groups of globular actin, or G-actin, with AlexaFluor 488 carboxylic acid succinimidyl ester, resulting in a dye/protein ratio of 0.6 (2). G-actin labeled with biotin was purchased from Cytoskeleton. Monomeric actin containing 10%, 20%, or 30% labeled Alexa 488 actin and 0.25% of biotinylated actin is stored in G Buffer (2 mM Tris, 0.2 mM $CaCl_2$, 0.2 mM DTT, 0.2 mM Na_2ATP at pH 8.0). Myosin II is purified from rabbit skeletal muscle as previously described (3), and its functionality is confirmed by motility assays showing an average gliding speed of 4.5 ± 1.5 μm/s (n = 27) (4). Fluorescent myosin is prepared by labeling amine groups with Dy-Light 594 NHS ester. Myosin filaments are prepared by diluting the myosin stock against assembly buffer containing 50 mM KCl, resulting in filaments composed of about 100 myosin proteins and with an average length of 0.69 μm (5).

Liposome Formation (Outside Geometry). Unless noted otherwise, the osmolarities of the inside and outside buffer are matched. Liposomes are electroformed (6). Briefly, 20 μL of a mixture of EPC lipids and biotin PEG lipids (present at 0.1 or 1 mol %, respectively, for weak and strong attachment) with a concentration of 2.5 mg/mL in chloroform/methanol 5:3 (vol:vol) are spread on Indium Tin Oxyde coated plates (ITO plates) and dried under nitrogen flow, then placed under vacuum for 2 h. A chamber is formed using the ITO plates (their conductive sides facing each other) filled with sucrose buffer (200 mM sucrose, 2 mM Tris adjusted at pH 7.4) and sealed with hematocrit paste (Vitrex Medical). Liposomes are formed by applying an alternate current voltage (10 Hz) for 1 h and 15 min.

Agarose Precursor Method (Inside Geometry). Liposomes are prepared using a procedure that combines two procedures: an agarose swelling method (7) and an inverse phase precursor method (8). Agarose (Type IX-A) is dissolved at 1% (wt/wt) in deionized water and 300 μL is spin-coated at 1,200 rpm for 30 s on 24 × 24 mm glass coverslips and dried for 30 min at 37 °C. Membranes were composed of DOPC, always doped with 2.5 or 5 mol% PEG-PE to prevent nonspecific protein adhesion. We obtained equivalent results when using 2.5 or 5 mol% PEG lipids for both the actin shell characterization and the examination of myosin foci position inside liposomes. "Weak attachment" conditions correspond to 0 mol% biotin-PE and 5 mol% PEG-PE, whereas "strong attachment" conditions correspond to 2 mol% biotin-PE and 2.5 mol% PEG-PE. Membranes were sometimes doped with either 0.2 mol% rhodamine-PE, for fluorescence imaging in the absence of myosin, or 0.2 mol% Pacific Blue-PE, for imaging in the presence of myosin. Lipids are dissolved in 95:5 (vol/vol) chloroform/methanol at 3.75 mg/mL. An inverted phase of water droplets in the lipid solution is formed by adding 3.5 μL of a neutravidin solution (48 mg/mL in PBS) or just PBS to 60 μL of the lipid mixture. The mixture is pipetted up and down until opalescence, indicating that inverted micelle precursors have formed. The micelles (40 μL) are spin-coated at 100 rpm for 100 s on agarose slides and then dried under vacuum for 100 min at room temperature. An open-top formation chamber is assembled by placing a 0.12 mm thick spacer (secure-seal spacer; Invitrogen) on the lipid-coated slide. An inner buffer (I buffer) containing actin and myosin proteins is pipetted on top of the formation chamber and incubated for 90 min at 4 °C to form liposomes. Liposomes are collected by pipetting ~three volumes of O buffer (glucose solution) into the formation chamber and tilting the slide to flow the liposomes into an open-top observation chamber assembled from a glass slide and a 0.5 mm thick spacer (Coverwell; 13 mm in diameter; Invitrogen). Then, the observation chamber is closed to avoid evaporation. Glass slides are passivated by 2 mg/mL casein. The O buffer osmolarity is adjusted be 15 mOsmol higher than the I buffer osmolarity to prevent liposome rupture (Osmomat 030; Gonotec). We confirmed the functionality of neutravidin by two observations: (*i*) fluorescent neutravidin localizes to the membrane only when biotinylated lipids are present (compare Fig. S10 *A* and *B*); and (*ii*) fluorescent biotin only binds to the inner leaflet of the membrane when neutravidin is bound there (compare Fig. S10 *C* and *D*).

Observation of Liposomes (Outside Geometry). Epifluorescence and phase contrast microscopy are performed using an IX70 Olympus inverted microscope with a 100× or a 60× oil immersion objective. Spinning disk confocal microscopy is performed on a Nikon Eclipse T1 microscope with an Andor Evolution scan head and a 60× water immersion objective. Observation chambers are made by heating two Parafilm strips (as spacer) between two coverslips. Randomly chosen liposomes are imaged over time. Kymographs and intensity profiles are made using Image J. The speeds of actin contraction are measured on kymographs (along a line on the liposome for the crushing or along the contour of the fluorescent actin shell for the peeling) by the slopes of the intensity traces of binarized intensity of fluorescent actin (Fig. 3 *B* and *D*).

Observation of Liposomes (Inside Geometry). Liposomes with encapsulated actin and myosin are observed with a confocal laser scanning microscope using a Nikon EZC1 scan head on a Nikon Eclipse Ti inverted microscope with 100× plan Apo objectives.

Image Analysis (Outside Geometry). Epifluorescence and confocal microscopy images are used to extract intensity profiles along a radius starting from the center of the liposome and averaged around each liposome. The actin shell thickness is measured as the distance between the point of maximal actin fluorescence intensity and the point where the fluorescence intensity decays to half of the maximal value, similar to a procedure used previously for actin shells anchored to beads (9). The mean fluorescence intensity I_{MEAN} is measured on the liposome contour with a line

width of 10 pixels and the fluorescence background, $I_{background}$, is measured on a dark area of the image. The quantity $\Delta I_m = (I_{MEAN} - I_{background})/I_{background}$ provides a relative measure of the adsorption of actin on the outer leaflet of liposome membranes for different attachment conditions. After 15 min incubation with actin filaments, liposomes with 1% or 0.1% biotinylated lipids show the same actin adsorption i.e., the same value of ΔI_m around 0.2. Even though epifluorescence images include fluorescence outside the focal plane, image deconvolution does not change the measured thickness values or ΔI_m.

Image Analysis (Inside Geometry). The actin shell thickness is determined by integrating the fluorescence intensity around concentric circles and repeating this for radial distances from the liposome center to the liposome edge. By normalizing all values by the corresponding circumference (in pixels), we obtain a profile of integrated intensities along the liposome radius. To compare the integrated intensities of a liposome, we normalize each integrated intensity by subtracting the minimum integrated intensity and then dividing by the difference between the maximum and minimum integrated intensities. The actin shell thickness is defined as the distance between the liposome edge and the radial position where the normalized integrated intensity is greater than 0.5. The shell thickness is finally divided by the liposome radius to obtain a normalized shell thickness. For a homogeneously filled liposome, we expect a normalized shell thickness of 1. Because thick actin shells are, in practice, difficult to distinguish from homogeneous networks, we define liposomes with a normalized shell thickness above 0.7 as "bulk" and liposomes with normalized shell thicknesses below 0.7 as exhibiting a cortical actin shell The average actin intensity is obtained by summing fluorescence intensities of all pixels inside the liposome and dividing the sum by the total number of pixels. To compare encapsulation efficiencies for a population of liposomes examined under identical illumination conditions, we normalize the average intensity of each by the maximum value of the distribution. We exclude liposomes from the analyses which contained lipid structures such as tubes, lipid aggregates, or small liposomes (typically present in around 50% of all liposomes). To quantify the position of myosin foci after active cortex contraction, we use confocal fluorescence z stacks of the actin and myosin signals inside the liposomes. To determine the 3D contour of the liposomes, we fit the actin signal in each plane of the z stack to an ellipse. The resulting stack of ellipses is then fitted to an ellipsoid and its center position and radius are determined. We then manually locate the position of the myosin cluster and measure its distance from the center of the ellipsoid (D_{myo}). Finally, we calculate the relative distance of the myosin cluster normalized by the radius of the liposome as $D_{myo}/R_{liposome}$.

1. Pardee JD, Spudich JA (1982) Purification of muscle actin. *Methods Cell Biol* 24: 271–289.
2. Gentry BS, et al. (2012) Multiple actin binding domains of Ena/VASP proteins determine actin network stiffening. *Eur Biophys J* 41(11):979–990.
3. Margossian SS, Lowey S (1982) Preparation of myosin and its subfragments from rabbit skeletal muscle. *Methods Enzymol* 85(Pt B):55–71.
4. Toyoshima YY, et al. (1987) Myosin subfragment-1 is sufficient to move actin filaments *in vitro*. *Nature* 328(6130):536–539.
5. Soares e Silva M, et al. (2011) Active multistage coarsening of actin networks driven by myosin motors. *Proc Natl Acad Sci USA* 108(23):9408–9413.
6. Angelova M, Dimitrov D (1986) Liposome electroformation. *Faraday Discuss Chem Soc* 81:303–311.
7. Tsai FC, Stuhrmann B, Koenderink GH (2011) Encapsulation of active cytoskeletal protein networks in cell-sized liposomes. *Langmuir* 27(16):10061–10071.
8. Mertins O, da Silveira NP, Pohlmann AR, Schröder AP, Marques CM (2009) Electroformation of giant vesicles from an inverse phase precursor. *Biophys J* 96 (7):2719–2726.
9. van der Gucht J, Paluch E, Plastino J, Sykes C (2005) Stress release drives symmetry breaking for actin-based movement. *Proc Natl Acad Sci USA* 102(22):7847–7852.

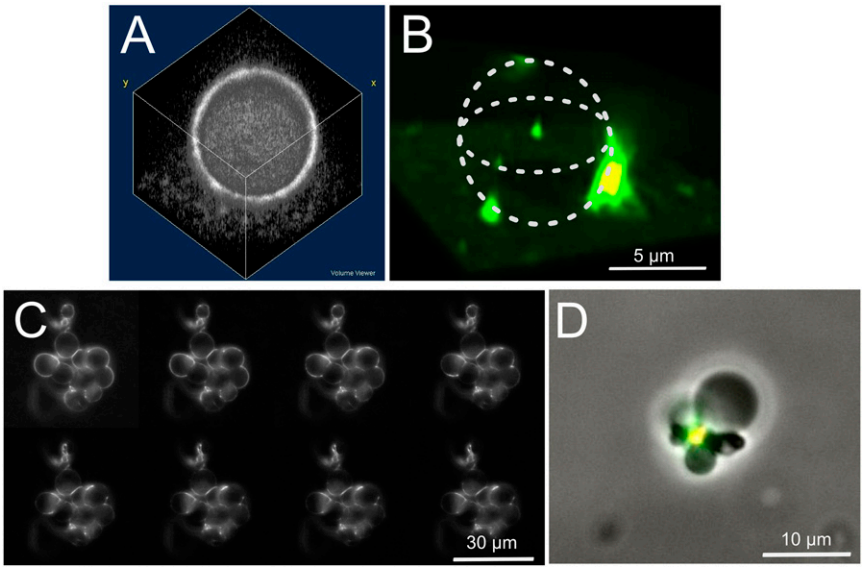

Fig. S1. Three-dimensional reconstruction of an actin-decorated liposome in the outside geometry (*A* and *B*). (*A*) Spinning-disk confocal microscopy observation of fluorescent actin filaments anchored on the outer leaflet of a liposome membrane. The shell is homogeneous before myosin addition. The size of the 3D visualization box is 25 µm × 25 µm × 15 µm, respectively, on the *x*, *y*, and *z* axis. (*B*) Spinning-disk confocal microscopy observation of fluorescent actin (green) and fluorescent myosin (red). Actin is peeled toward one pole. (*C* and *D*) "Undetermined" cases of contraction. (*C*) Epifluorescence images of fluorescent actin peeling during a time lapse movie (one frame per minute) of a contracting aggregate of multiple (~10) liposomes. (*D*) Superposition of phase contrast image with epifluorescence image of actin (green) and myosin (red) at the end of an experiment of one undetermined case. We refer to the situations (*C* and *D*) as undetermined in Fig. 3.

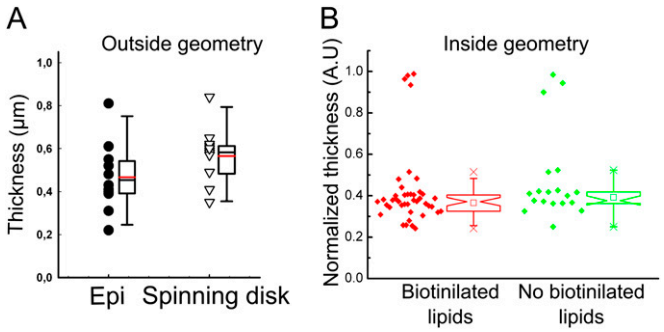

Fig. S2. Thickness distributions of actin shells. (*A*) Thickness of actin shells in the outside geometry measured by epifluorescence microscopy (black circles) or spinning disk confocal microscopy (white triangles) for 20 liposomes. The lower boundary of the box plot indicates the 25th percentile, a black line within the box marks the median and a red line marks the mean, and the upper boundary of the box indicates the 75th percentile. The whiskers indicate the 90th and 10th percentiles. (*B*) Thickness of actin shells in the inside geometry (normalized by liposome radius) in the presence (red symbols) or absence (green symbols) of biotinylated lipids. We define liposomes with a normalized shell thickness above 0.7 as bulk. Box plots were computed only for the liposomes that exhibit a shell (i.e., with a normalized shell thickness below 0.7). The box plots show the mean value (small squares) the median value (notches), maximum and minimum values (crosses), and 5th and 95th percentiles (whiskers). The lower boundary of the box plot indicates the 25th percentile and the upper boundary indicates the 75th percentile of the populations (42 and 19 liposomes for the strong and weak anchoring cases, respectively).

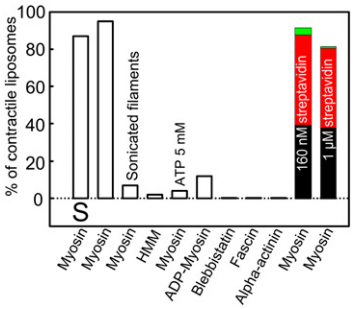

Fig. S3. Percentage of contractile liposomes in different experimental conditions. The molar percentage of biotinylated lipids is 0.1% for weak attachment and 1% for strong attachment (S below the bars). At least 30–50 liposomes were analyzed in all cases except for myosin strong attachment (391 liposomes) and myosin weak attachment (150 liposomes). Myosin II filaments are replaced by myosin II subfragments (HMM), myosin II filaments with reduce motor duty ratio are replaced by an excess of ATP (5 mM instead of 1 mM), inactive ADP-myosin filaments and inhibited myosin II filament are replaced by the specific drug blebbistatin, or myosin is replaced by the passive physiological cross-linker fascin or α-actinin. We observe contraction only very rarely or not at all in these control cases similarly to bulk actomyosin contraction, contraction of the quasi-2D–anchored cortex requires the organization of myosin motors into bipolar filaments and sufficient motor processivity. For the conditions with 160 nM myosin and 1 μM streptavidin, we distinguish between the fraction of liposomes crushing (black), peeling (red), and undetermined cases (green).

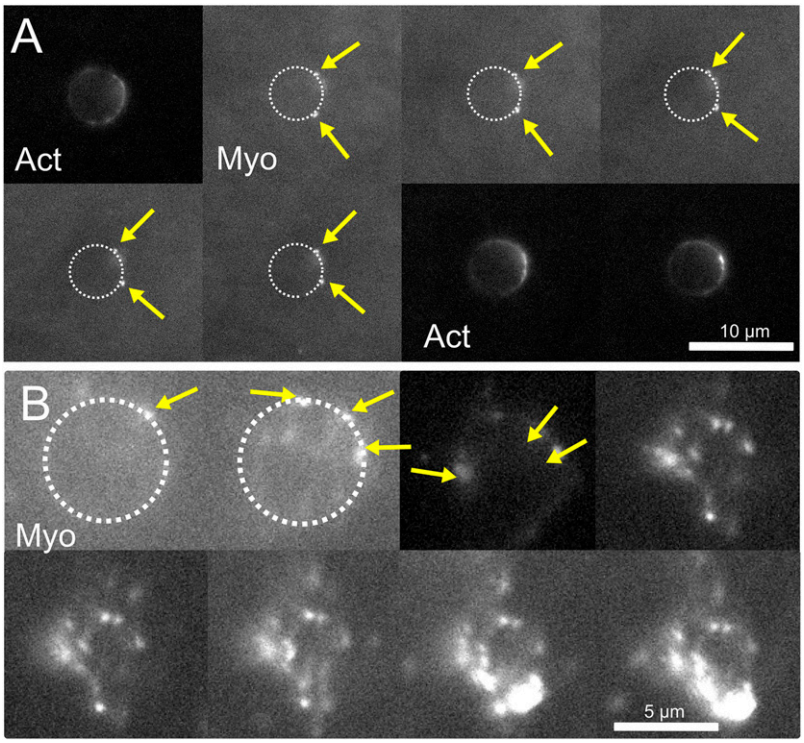

Fig. S4. Myosin binding and subsequent redistribution during cortex peeling and liposome crushing case after injection of fluorescent myosin next to a liposome carrying an actin shell. (*A*) Epifluorescence images of actin (labeled "Act" in *Inset*) or myosin (labeled "Myo" in *Inset*) at one frame per minute of a peeling cortex where we can detect the position of the myosin spot and visualize the peeling process of actin. (*B*) Epifluorescence time lapse image of fluorescent myosin during a crushing event of a liposome at one frame every 40 s. The movement starts once two or three myosin foci (yellow arrows) are bound to the actin shell (24 liposomes altogether, average value of 2.8 ± 1.7 myosin spots, and extremum values of one and five spots).

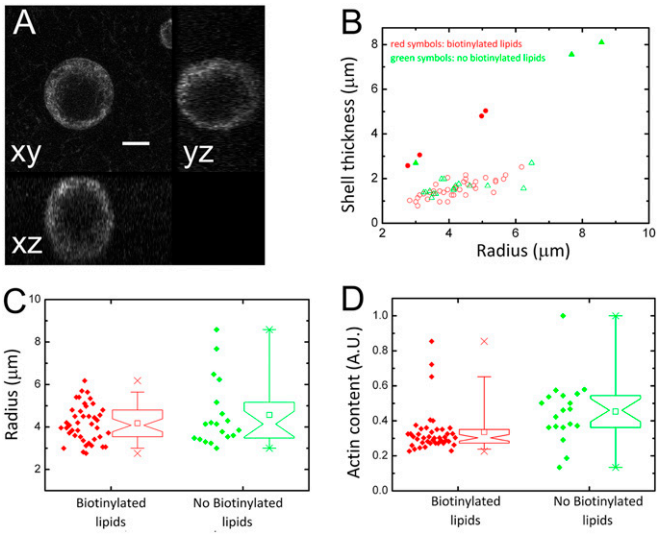

Fig. S5. Characterization of the actin content inside liposomes. (*A*) Three-dimensional image reconstruction (in the form of *x-y*, *y-z*, and *x-z* sections) of a liposome with an actin shell anchored to the inner leaflet of the membrane by biotin-neutravidin linkages. The actin shell is homogeneous. (Scale bar: 5 μm.) (*B*) Dependence of actin shell thickness on liposome radius. Empty symbols denote liposomes exhibiting actin shells and solid symbols denote liposomes filled with a bulk actin network. (*C*) Notched box plot of liposome radius in the two different conditions as indicated. (*D*) Notched box plot of actin content, normalized by the maximum actin intensity of the distribution. The box plots show the mean value (small squares), the median value (notches), maximum and minimum (crosses), and 5th and 95th percentiles (whiskers). The lower boundary of the box plot indicates the 25th percentile and the upper boundary indicates the 75th percentile of the populations (42 and 19 liposomes for the strong and weak anchoring cases, respectively).

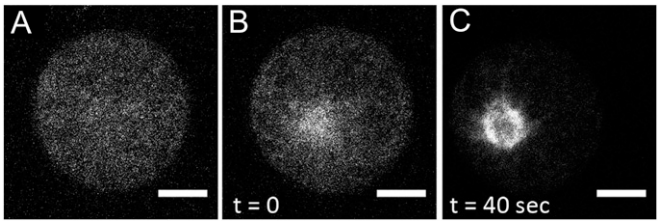

Fig. S6. Kinetics of contraction in the inside geometry. To permit immediate visualization of contraction upon myosin activation, we heated the sample on the microscope stage from 4 to 20 °C using a dedicated temperature stage. At 4 °C, actin was homogeneously distributed inside the liposome as seen in *A*. Directly upon heating to 20 °C, signatures of network contraction are already visible (*B*). After 40 seconds at 20 °C, the actin network has already contracted inwards, away from the membrane (*C*). (Scale bars: 5 μm.)

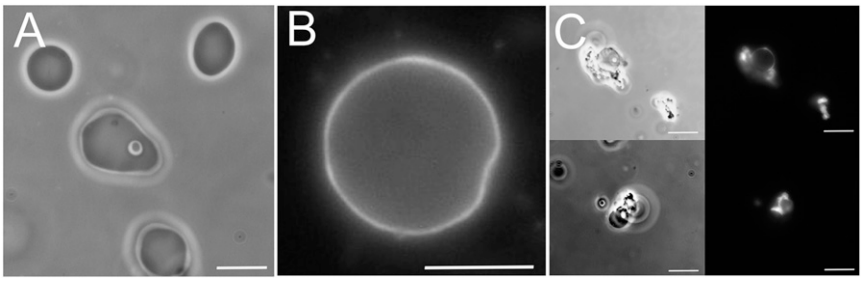

Fig. S7. Osmotically deflated liposomes are always crushed after injection of myosin. (*A*) Phase-contrast image of deflated liposomes by an increase of osmolarity of 40 mOsm in the outside buffer in absence of actin and myosin. (*B*) Epifluorescence image of fluorescent actin linked to a liposome membrane before myosin minifilament injection in the chamber. Because of the osmotic pressure, the liposomes do not appear perfectly round but deformed by the addition of actin filaments. (*C*) Phase-contrast images (*Left*) and epifluorescence images of actin (*Right*) 20 min after addition of 20 nM myosin. (Scale bars: 10 μm.)

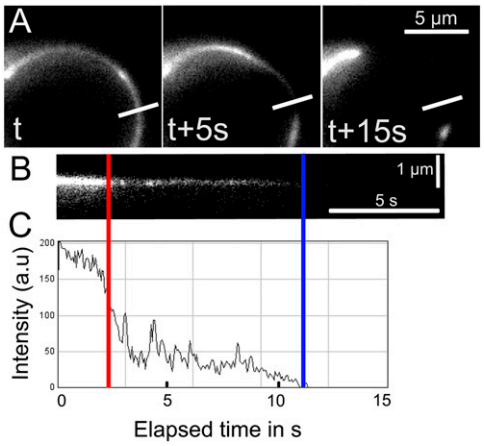

Fig. S8. During peeling, actin shells become thinner before they break (*A*–*C*). (*A*) Time-lapse image sequence of a peeling liposome (one frame every 10 s). (*B*) Kymograph along the line shown in *A* with corresponding scale bars. (*C*) Intensity profile of the kymograph. Red bar, the actin shell starts to appear thinner; blue bar, time point t_{AM} as defined in *Results*, where the network breaks, as evidenced by the disappearance of actin fluorescence. This is a representative example from a set of 15 independent experiments on different liposomes.

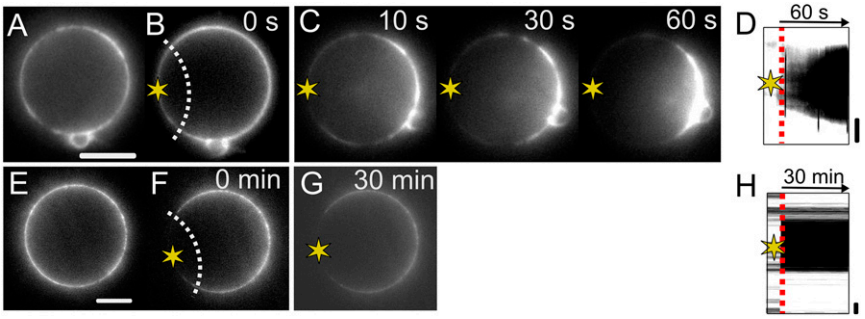

Fig. S9. Peeling can be artificially triggered under strong attachment conditions (that would normally promote liposome crushing) by locally photodamaging the actin network. (*A–D*) Peeling in the presence of myosin. (*E–H*) Control vesicle in the absence of myosin. In both cases, epifluorescence images (*A–C*, *E–G*) are shown side-by-side with corresponding kymographs constructed along the liposome contour (*D* and *H*). The yellow star on the images (*B*, *C*, *F*, and *G*) represents the center of the photodamaged region on the membrane visualized by the white dashed line, which represents the center the kymographs. The red dashed line in the kymographs represents the starting time of photodamaging. (*A* and *E*) Liposome before photobleaching. (*B* and *F*) Liposomes after photodamaging the actin shell. In *D*, time 0 corresponds to the time of injection of 200 nM myosin II minifilaments in the chamber, whereas in *H*, time 0 corresponds to the injection of buffer only. (*C* and *D*) In the presence of myosin, peeling occurs with an average velocity of 10.5 ± 1.8 μm/min (four liposomes). In the control experiments, no peeling is observed (10 liposomes). (Scale bars: 10 μm.)

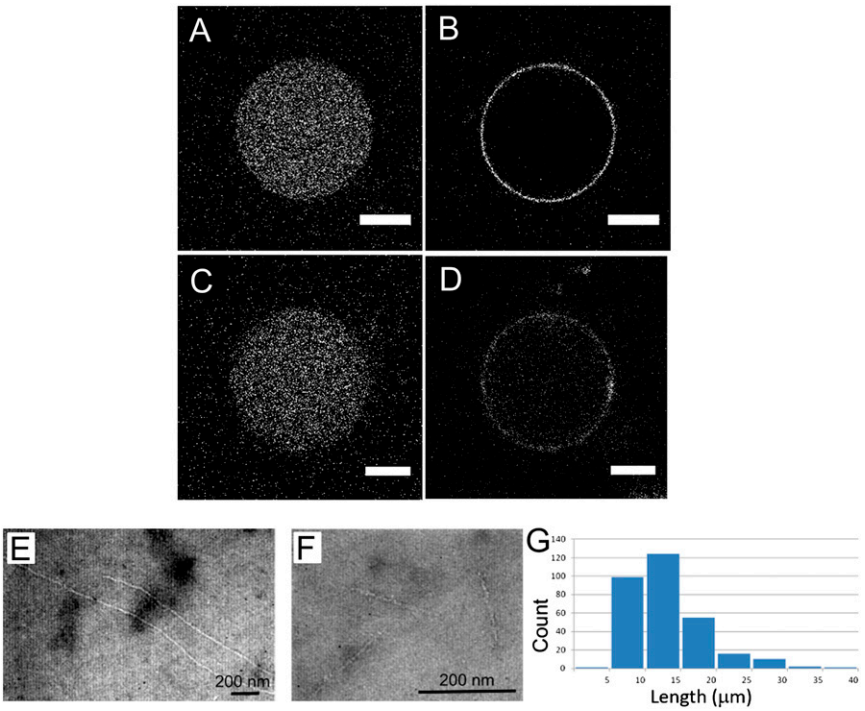

Fig. S10. Confocal fluorescence micrographs of liposomes produced by the agarose-precursor method (*A–D*). To assess the specificity of binding of biotinylated lipids to neutravidin, neutravidin labeled with AlexaFluor 350 is incorporated into the inverse phase precursor micelles either in the absence (*A*) or presence (*B*) of biotinylated lipids. To test that neutravidin is still functionally active after the inverse phase precursor procedure, we encapsulate biotin-fluorescein into the liposomes in the absence (*C*) or presence (*D*) of neutravidin on the membrane. Concentrations of biotin-fluorescein are 50 and 500 nM for liposomes in *C* and *D*, respectively. (Scale bars: 5 μm.) Length distribution of actin filaments (*E–G*). (*E*) Negatively stained electron microscopy images of actin filaments used for making actin shells in the outside geometry. The average filament length is 4 μm (30 filaments). (*F*) EM image of actin filaments shortened by 5-min sonication, which reduces the average length to 0.2 μm (n = 50). (*G*) Length distribution of actin filaments used for making shells in the inside geometry, measured by fluorescence microscopy of dilute filaments (10 nM, including 5% Alexa 488-labeled actin) stabilized by phalloidin (1:1 molar ratio to actin). The average length is 13 ± 5 μm (n = 307).